Cell Mol Neurobiol (2008) 28:389–409
DOI 10.1007/s10571-007-9255-9

ORIGINAL PAPER

Effects of Disrupting Calcium Homeostasis on Neuronal Maturation: Early Inhibition and Later Recovery

Sarah L. Ringler · Jamie Aye · Erica Byrne · Megan Anderson · Christopher P. Turner

Received: 23 September 2007 / Accepted: 14 December 2007 / Published online: 15 January 2008

Abstract It has become increasingly clear that agents that disrupt calcium homeostasis may also be toxic to developing neurons. Using isolated primary neurons, we sought to understand the neurotoxicity of agents such as MK801 (which blocks ligand-gated calcium entry), BAPTA (which chelates intracellular calcium), and thapsigargin (TG; which inhibits the endoplasmic reticulum Ca^{2+}-ATPase pump). Thus, E18 rat cortical neurons were grown for 1 day in vitro (DIV) and then exposed to vehicle (0.1% DMSO), MK801 (0.01–20 μM), BAPTA (0.1–20 μM), or TG (0.001–1 μM) for 24 h. We found that all three agents could profoundly influence early neuronal maturation (growth cone expansion, neurite length, neurite complexity), with the order of potency being MK801 < BAPTA < TG. We next asked if cultures exposed to these agents were able to re-establish their developmental program once the agent was removed. When we examined network maturity at 4 and 7 DIV, the order of recovery was MK801 > BAPTA > TG. Thus, mechanistically distinct ways of disrupting calcium homeostasis differentially influenced both short-term and long-term neuronal maturation. These observations suggest that agents that act by altering intracellular calcium and are used in obstetrics or neonatology may be quite harmful to the still-developing human brain.

Keywords Neurite · Growth cone · Glutamate · Calcium · Development · Morphology

Introduction

The postnatal period represents a time when the brain is actively establishing or fine-tuning its circuitry prior to attaining adult-like stability (Rice and Barone 2000; Levitt 2003) and

S. L. Ringler · J. Aye · E. Byrne · M. Anderson · C. P. Turner (✉)
Neurobiology & Anatomy, Wake Forest University Medical School, Medical Center Boulevard, Winston Salem, NC 27157-1010, USA
e-mail: cpturner@wfubmc.edu

disruption of this activity may promote pathological changes that result in altered network organization. Maintaining calcium homeostasis during the postnatal period may be critical to still-developing neurons as blockade of calcium entry through the *N*-methyl-D-aspartate receptor (NMDAR; a calcium permeant ion channel), or voltage-operated calcium channels, can induce caspase-3-dependent apoptosis in postnatal day 7 (P7) rats (Turner et al. 2007b). Injury was found in neurons that did not express the calcium-binding proteins (CaBPs) calbindin-D28K, calretinin, or parvalbumin (Lema Tomé et al. 2006, 2007), suggesting that still-developing neurons less able to regulate calcium homeostasis may be vulnerable to agents that alter intracellular calcium.

The postnatal period in rats (equivalent to the last trimester, first 1–2 years in humans) is associated with stage-specific changes in neuronal maturation. These include early axon and dendritic growth (directed by dynamic changes in growth cones and filopodia), followed by increased arborization of these processes, as well as peaks in synaptogenesis and myelination (Herschkowitz 1988; Takashima et al. 1995; Rice and Barone 2000; Levitt 2003). Likewise, in vitro neuronal maturation progresses in stages (Dotti et al. 1988; Fletcher and Banker 1989; Fletcher et al. 1994; Santama et al. 1996). For example, the initial period of growth cone-directed neurite elongation is quickly followed by neurite polarization (emergence of tau-positive axons and MAP2-positive dendrites) and arborization (Bradke and Dotti 1999, 2000). By 7 days in vitro (DIV), formal networks of neuronal fibers have been established and these continue to mature, displaying a surge in synaptogenesis at later times. Whereas it must be understood that neuronal development in vitro is not a faithful recapitulation of in vivo maturation (Chilton and Gordon-Weeks 2006), the ontological progress of neurons in both environments is driven by common stage-specific events. For example, changes in NMDAR subunit or CaBP expression follow similar in vitro and in vivo patterns that appear to be linked to specific stages of neuronal maturation (Zhong et al. 1994; Tucker and Morton 1995; Zhong et al. 1995; Cheng et al. 1999; Hoffmann et al. 2000; Ming et al. 2002).

To more fully understand the influence of calcium on neuronal maturation, we exposed primary neuronal cultures to the NMDAR antagonist MK801 (which blocks calcium entry) and for comparison, to two mechanistically distinct agents, BAPTA (an intracellular calcium chelator) and thapsigargin (TG; an endoplasmic reticulum (ER) Ca^{2+}-ATPase pump inhibitor). All three agents reduced active growth cone numbers, as well as neurite length and complexity and, at later in vitro times, prevented the establishment of neuronal networks. The potency of inhibition was found to be MK801 < BAPTA < TG, suggesting that neuronal development can be blocked by altering intracellular calcium levels in mechanistically diverse ways. Increasingly, agents that regulate calcium entry or homeostasis are used in obstetrics, neonatology, or as drugs of abuse in pregnant women, suggesting the findings we present here may be relevant to clinical and pathological situations associated with the late gestational period or the first 1–2 years of human life.

Methods

Primary Neuronal Cultures

The use of animals in this study was approved by the Wake Forest Animal Care and Use Committee in accordance with NIH guidelines. Unless otherwise stated all reagents were purchased from Sigma-Aldrich (St Louis, MO). Cortical neurons were obtained from E18 Sprague-Dawley rat embryos (Charles Rivers, Charlotte, NC) which were removed under 2% isofluorane anesthesia. The cortical lobes of 10 brains were separated from subcortical

structures in calcium-magnesium-free, Hank's balanced salt solution containing 1 mM sodium pyruvate and 10 mM HEPES buffer (Invitrogen, Carlsbad, CA). After removal of meninges, brain tissue was placed into Hibernate E (Brain Bits, Springfield, IL) supplemented with B27 (Invitrogen), triturated briefly, and incubated at 37°C for 5 min with 2.5% trypsin (Invitrogen) and deoxyribonuclease I (Type IV). Cells were then further dissociated mechanically and centrifuged at 590 rpm, at 4°C for 5 min. The pellet was resuspended in Neurobasal Media (NBM; supplemented with glutamate, glutamine, antibiotic-antimicotic solution, and B27). Cells were plated at a density of approximately 35,000 cells/well on poly-D-lysine-coated glass coverslips (Fisher, Pittsburgh, PA) in 24-well plates (Corning Inc; Corning, NY). After 1 day in vitro (DIV), 50% of the media was replaced with glutamate-free NBM and cells were fed with the same NBM every 3 days thereafter, as required.

Agents and Treatments

Neurons were treated with either vehicle (dimethyl sulfoxide (DMSO), final concentration of 0.1%), or one of the following in DMSO: the NMDAR antagonist MK801 (dizocilpine; 0.01, 0.1, 1, 10 or 20 μM), the calcium chelator 1,2-Bis(2-aminophenoxy)ethane-*N,N,N′,N′*-tetra-acetic acid-acetoxymethyl ester (BAPTA-AM; 0.1, 1, 2, 10, or 20 μM; Invitrogen, Eugene, OR), or the Ca^{2+}-ATPase pump inhibitor thapsigargin (TG; 0.0001, 0.001, 0.01, 0.1, or 1 μM). In addition, cells were exposed to the nicotinic agonist nicotine (1–100 μM), the nicotinic antagonist mecamylamine (1–100 μM), or the NMDAR receptor agonist NMDA (10 μM) in the absence or presence of MK801 (10 μM).

Cultures were plated as described (above) and grown for 1 DIV. Vehicle or agents were added for 24 h (at the concentrations indicated above) and cultures were either fixed and stained for various markers (see below) or agents were removed by replacing media with agent-free media and cultures allowed to recover until 4 or 7 DIV. To avoid drying out, media changes were performed 4 wells at a time. At 4 or 7 DIV, cultures were then fixed and stained for various markers (see below).

Cell Staining

After exposure to agents (see above), cells were fixed by adding 4% PFA in PBS to each well (pre-warmed to 37°C; 2% effective concentration) and the plates returned to the 37°C incubator for 15 min. Cells were then washed three times with PBS and incubated with a rabbit anti-tau, polyclonal antibody (1:4000; DakoCytomation, Carpenteria, CA) or a mouse anti-MAP2 monoclonal antibody (1:2000; Sigma-Aldrich, St Louis, MO) for 24 h (4°C), washed in PBS (×3), incubated with an AlexaFluor 488, goat anti-rabbit secondary antibody (1:200; Invitrogen) or AlexaFluor 488, donkey anti-mouse secondary antibody (1:200, Invitrogen) for 2 h at room temperature, washed with PBS (x3), incubated with rhodamine-conjugated phalloidin to label F-actin (1:40; Invitrogen), and washed again in PBS. Coverslips were then mounted onto glass slides using VectaShield (containing DAPI; Vector Labs, Burlingame, CA). For 4 and 7 DIV cultures, cells were fixed, stained for tau protein, and coverslipped (as above). In addition, parallel cultures (1 DIV) were stained for NR1, the obligatory NMDAR subunit, using a rabbit polyclonal antibody (1:200; Chemicon, Temecula, CA) and an AlexaFluor 488 goat-anti-rabbit secondary (1:200, Invitrogen). To determine neuronal from non-neuronal cells, cultures were labeled for neuronal nuclei using a mouse anti-NeuN monoclonal antibody (1:400; Chemicon) and AlexaFluor 488 donkey anti-mouse secondary.

Imaging and Image Analysis

Images of the same field were collected at 20 or 40× under UV light with filters selective for emission wavelengths of 461 nm (DAPI), 488 nm (tau, MAP2, NR1, NeuN), or 594 nm (F-actin), using an Olympus IX70 Inverted System Microscope (Olympus, Melville, NY), a Hamamatsu digital camera (Hamamatsu City, Japan), and IPLab 3.6.4 software (Scanalytics, Inc.; Fairfax, VA). Images were saved as TIFF files, imported into Adobe Photoshop 7.0 (Adobe Systems, Inc; San Jose, CA), and pseudo-colored blue for DAPI-labeled nuclei, green for tau, MAP2, NR1, or NeuN; or red for F-actin. Images were analyzed using Image Pro 5.0 (MediaCybernetics, Baltimore, MD). Please note that although images were captured at 20 or 40× magnification, Image Pro 5.0 has a local zooming feature that allows cellular details to be easily visualized and analyzed.

Growth Cones

Images were collected at 20× magnification as described above. We sampled only growth cones that were clearly expanded (EGCs), displaying a sheet-like lamellipodia with numerous filopodia (see Fig. 2). Growth cones with a shrunken lamellipodia and no filopodia were not counted. To account for field-to-field variations in cell number, growth cone numbers were normalized. In earlier studies, we had used a total growth cone-to-total DAPI ratio (large, weakly labeled nuclei) for the entire field but this approach assumed that all growth cones in the field were associated with all DAPI-labeled neuronal nuclei (which was not always the case). To eliminate this assumption we sampled only growth cones from neurites whose cell body could be unambiguously assigned to such neurites. To verify that the data derived were not dependent on a given morphological feature, we determined the EGC numbers per cell as well as the EGC numbers per process (all primary, secondary, and tertiary neurites were included in this estimation). The mean EGC number/cell or EGC number/process (±SE) was estimated from 20 to 30 cells, across 2 fields per well, and across 4 wells per treatment group.

Neurite Length

Images were collected at 20× as described above. Neurite length was estimated using an ImagePro 5.0 manual tracing feature (calibrated to display dimensions in microns) on rhodamine-phalloidin-labeled neurites. To facilitate tracing of processes, cultures were co-labeled with either anti-tau or anti-MAP2 antibodies so that regions not well labeled by rhodamine-phalloidin would be filled in by tau or MAP2 immunoreactivity. Only the length of primary neurites was determined (Fig. 3d), sampling from 2 fields per well across 4 wells per treatment group. Initial analysis revealed that, in vehicle-treated wells, a broad range of neurite lengths were observed. Thus, we expressed neurite length as the frequency of neurites that fell into the following dimensions: 10–30, 31–50, >50 μm.

Neurite Complexity

Images of F-actin labeled neurites were captured at 20× as described above. Co-labeling for tau or MAP2 was used to facilitate identification of processes. Neurite complexity was determined by counting the number of primary, secondary, and tertiary neurites for each cell. Only neurons whose soma and processes were in the captured image were sampled (excluded from the analysis were neurons whose processes extended beyond the field of view or

processes whose somas were located outside the captured image). Primary neurites were defined as processes projecting directly from the cell body, secondary neurites were processes that branched from any primary neurite and tertiary processes were those that projected from any secondary neurite (see Fig. 3d). Sampling was from 2 fields per well, across 4 wells per treatment group and data expressed as the mean (±SE) primary, secondary, or tertiary neurites per neuron.

Filopodial Per Unit Length of Neurites

Images were collected at 40× as described. F-actin labeled neurite filopodia were defined as processes shorter than the diameter of the neuronal cell body (processes longer than the soma diameter (>10 μm) were excluded from this analysis). We counted the number of filopodia along the length of each primary neurite and divided this number by the length of the neurite sampled. We limited our sampling to primary neurites. Sampling was from 2 fields per well, across 4 wells per treatment group and data expressed as the mean number of filopodia (±SE) per unit length of primary neurite.

Recovery-Fiber Density

Photomicrographs of tau-labeled processes were captured at 20× as described above. Images were imported into ImagePro 5.0, filtered first using the "Hi Gaussian" feature (7 × 7 setting) and then using the "Thinning" feature (threshold 20, passes 2, strength 10). This rendered the field of fibers as solid lines that faithfully reflected the outline of each process while maintaining a similar dimension (caliber) as the fibers in the original image. Pilot studies showed that the above procedure gave a skeleton version of each image that neither added additional information not found in the original image nor took away important information that would otherwise be included as data. After such skeletonization, a grid (grid file LineOrth.grd, width setting = 1; 15 horizontal × 15 vertical option) was superimposed onto the skeletonized image and the number of grid intersections made by the lines automatically counted (cultures with low-fiber density would intersect the grid far less than cultures with high-fiber density). This was repeated across 4 images per well and across 4 wells per treatment group. The mean number (±SE) of grid intersections per field was estimated for each treatment group.

Neuronal Numbers

Large, weakly labeled DAPI nuclei were consistently positive for the neuron-specific marker NeuN, whereas smaller, brighter nuclei were consistently NeuN-negative (see Fig. 1). In each field sampled and across all in vitro times studied (1, 4, 7 DIV), cells were routinely counterstained with DAPI and the mean number (±SE) of large weakly labeled nuclei (presumptive neurons) across 2 fields per well and across 4 quadruplicate wells for each treatment group was determined.

Statistics

Values were determined from a minimum of 2 fields per well across quadruplicate wells for each treatment group and are representative of data obtained from at least 3 independent cultures. For all analyses except neurite length, significant differences between the vehicle- and each of the agent-treated groups were determined using a one-way ANOVA with a Bonferroni post-test comparison of the means (significance at $P = 0.05$, 0.01, or 0.001, where

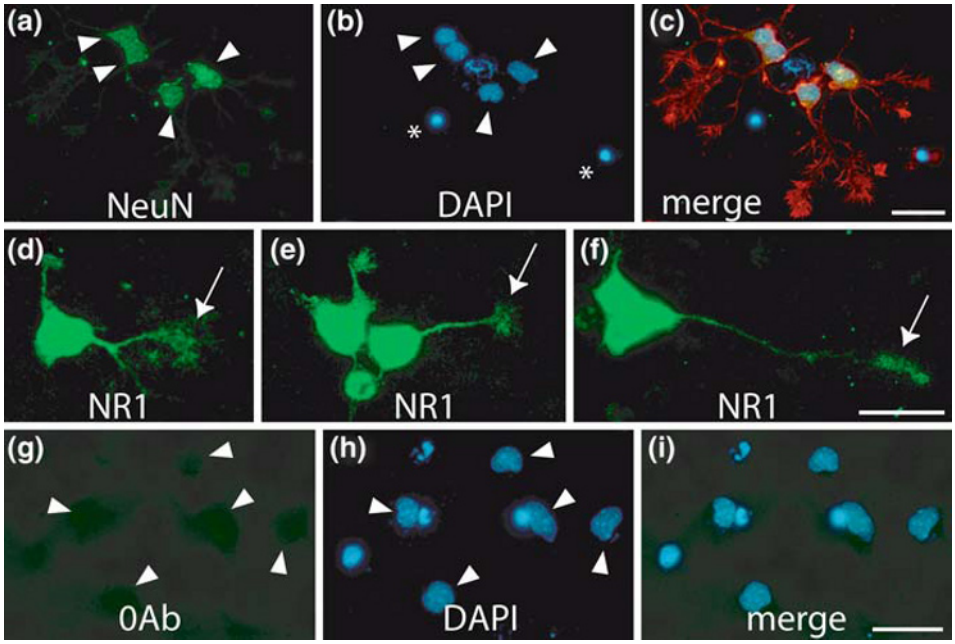

Fig. 1 Characterization of neuronal cultures. Neurons were grown for 1 DIV and stained for various proteins. (**a–c**). Cells in the same field were labeled with the neuron-specific marker NeuN (**a**), the nuclear dye DAPI (**b**), and the F-actin marker rhodamine-phalloidin (**c**). In **c**, all three markers are shown as a merged image. Arrowheads indicate the same cells co-labeled for NeuN (in **a**) and DAPI (in **b**); please note that only large, weakly stained, DAPI nuclei are NeuN-positive. Asterisks indicate DAPI-labeled cells that are small, bright, and NeuN-negative. (**d–f**) Parallel cultures were also stained for the NMDAR subunit, NR1. Each panel (**d–f**) shows various examples of NR1 staining; please note prominent labeling of growth cones (arrows). (**g–i**) Specific staining absent after omission of primary antibody. Arrowheads indicate absence of NR1 staining (**g**) in large, weakly labeled (DAPI) nuclei (**h**). Merged images shown in **i**. In panels where shown, scale bar is 30 μm

indicated). For neurite length, the data were best represented as a frequency distribution within various bin sizes (see above). Significant differences between vehicle- and agent-treated groups were determined using a χ^2-analysis within each bin size (significance at $P < 0.05$, where indicated). To test if there was an overall pattern within each bin size, a χ^2-test for trend was also performed (significance at $P < 0.05$, where indicated in text).

Results

Characterization of 1 DIV Cultures

Because all our studies started with primary cultures at 1 DIV, an important first step was to establish cell identity, as we had to be certain that we were consistently sampling from neurons and not other cells. When we stained 1 DIV cultures for the neuron-specific marker NeuN, nuclear staining was present in most cells in any given field (Fig. 1a). Counterstaining the same cultures with the nuclear dye DAPI revealed 2 morphologically distinct nuclei: large and weakly labeled; small and brightly labeled (Fig. 1b). The large weakly labeled nuclei were NeuN-positive (arrowheads) but the small bright nuclei were NeuN-negative (asterisks), suggesting the larger nuclei were neuronal. As a further indication that the large weakly labeled nuclei were neuronal, F-actin staining revealed that elaborate extensions and growth

cones emanated only from cells with such nuclei (Fig. 1c). Thus, we limited our analyses to processes that were clearly associated with large weakly stained (DAPI) nuclei.

In addition, because we later describe the action of MK801 on 1 DIV neurons, it was important to establish if the NMDAR was indeed present. We therefore stained 1 DIV cultures for the obligatory NR1 subunit (see Methods). We found NR1 staining was evident in the majority of 1 DIV neurons. Importantly, we noted prominent staining on the growth cones of these neurons (Fig. 1d–f). Omission of the primary antibody revealed staining was specific (Fig. 1g–i). Thus, in later studies, when we describe observations concerning MK801, we are confident that NMDAR expression is present in 1 DIV cultures.

Growth Cones

We next examined agent effects on expanded growth cones (EGCs). EGCs are characterized by flattened, expansive lamellipodia from which extend numerous motile filopodia. They are thought to be more sensitive to changes in the local environment and regulate path-finding activity (Gallo and Letourneau 1999). In contrast, inactive growth cones are club-shaped, or collapsed, have few to zero filopodia, and are seen during neurite retraction and cessation of outgrowth. Because we only sampled EGCs (see Fig. 2), we believe that in the following study we have quantified growth cones that could best be characterized as active (see Methods).

To determine agent-induced action on EGCs, primary neuronal cultures were grown as described (see Methods) and EGC numbers quantified following agent exposure. Thus, after 1 DIV, neurons were exposed to vehicle (0.1% DMSO), the NMDAR antagonist MK801

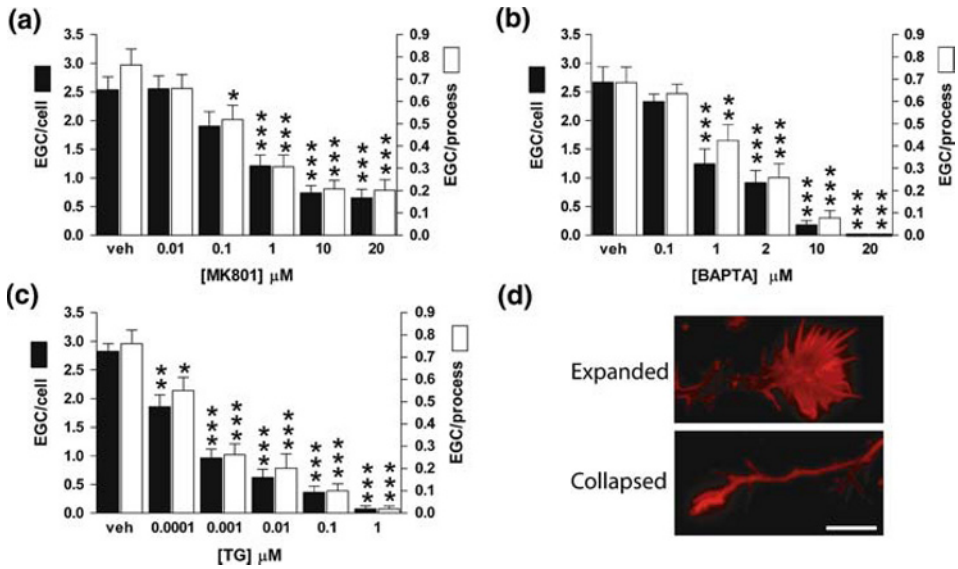

Fig. 2 Agent-induced loss of expanded growth cones. Neurons were grown for 1 DIV and exposed to varying concentrations of (**a**) MK801 (0.01–20 μM), (**b**) BAPTA (0.1–20 μM), or (**c**) thapsigargin (TG; 0.0001–1 μM) for 24 h. After fixing and staining for F-actin (see Methods), the number of expanded growth cones per cell (EGC/cell; see **d**—top panel) as well as the number of expanded growth cones per process (EGC/process) was estimated and the means (±SE) for each treatment group determined. Differences were assessed by ANOVA using a Bonferroni post-test comparison of means (* $P < 0.05$; ** $P < 0.01$; *** $P < 0.001$). (**d**) Top panel—expanded growth cone with numerous filopodia; bottom panel—collapsed growth cone (scale bar in the lower panel is 10 μm)

(10 nM–20 μM), the intracellular calcium chelator BAPTA-AM (100 nM–20 μM), or the ER Ca^{2+}-ATPase pump inhibitor TG (100 pM–1 μM) for 24 h. After this time, cells were stained for the cytoskeletal protein F-actin and captured images imported into ImagePro 5.0 for further analysis (See Methods).

After 24 h exposure to vehicle, cultures contained numerous cells with processes that frequently terminated in large growth cones which displayed expansive sheet-like lamellapodia with active filopodia projecting from the edge of the sheet (see Fig. 2d, upper panel). Less numerous were either processes that terminated in a bullet-like growth cone with no filopodia or processes with no growth cones at all (Fig. 2d, lower panel).

Cultures exposed to MK801 showed decreased numbers of EGCs with increasing concentration (Fig. 2a). The lowest concentration we observed an effect at was 100 nM (mean EGC/process; though not the mean EGC/cell). However, at higher concentrations a steady decline in the mean EGC/cell and mean EGC/process was observed, suggesting that the manner by which EGCs were assessed was not a major factor in determining outcome. With respect to cytosolic calcium, although significant changes were not observed until 1 μM BAPTA, the loss of EGCs at this and higher concentrations was much greater than at similar levels of MK801. When the influence of ER calcium was addressed, TG-induced inhibition of EGCs was evident even at the lowest concentration (100 pM). Thus the order of potency was MK801 < BAPTA < TG, indicating that the principal feature used by maturing neurons to guide the growth and elaboration of their processes (the growth cone) is inhibited by agents that disrupt calcium homeostasis. Although these results suggest that ER calcium may be more important to active growth cones than calcium entry or cytosolic calcium, differences in agent activity, compartmentalization, or affinity for their target(s) may ultimately determine overall efficacy.

It could be argued that, for MK801, effects on growth cones may be mediated through non-NMDARs, specifically the nicotinic ACh receptor (Ramoa et al. 1990). However, neither a specific agonist (nicotine; 1–100 μM) nor a selective antagonist (mecamylamine; 1–100 μM) influenced growth cones in the manner described above (mean EGC/cell: vehicle = 2.50 ± 0.51; nicotine 1 μM = 2.48 ± 0.19, 10 μM = 2.30 ± 0.11, 100 μM = 2.33 ± 0.16; mecamylamine 1 μM = 2.67 ± 0.22, 10 μM = 2.79 ± 0.27, 100 μM = 3.37 ± 0.32; not significant, ANOVA). Further evidence that MK801 was acting through the NMDAR was provided by the ability of MK801 to inhibit an NMDA-induced increase in EGCs (mean EGC/cell: vehicle 2.48 ± 0.15; 10 μM NMDA = 4.87 ± 0.66*; 10 μM NMDA plus 10 μM MK801 = 2.67 ± 0.09*; *P<0.05 comparing NMDA alone to vehicle or NMDA plus MK801 to NMDA alone, ANOVA).

Neurite Length

During the early stages of in vitro development, neurons grow processes quite rapidly, extending neurites across the substrate in search of new connections. Thus, 1 DIV cultures were exposed to vehicle, MK801, BAPTA, or TG for 24 h as described earlier and stained for the cytoskeletal marker F-actin to identify processes (see Methods). To facilitate tracing of processes, cultures were co-stained for tau or MAP2 proteins (not shown). We measured neurite length as described (see Methods) and found that length varied considerably even for the vehicle-treated cells and therefore expressed length as the frequency of neurites that fell into a specific bin size. Using bin sizes of 10–30, 31–50, and >50 μm, neurite length for vehicle-treated neurons tended to favor the larger bin sizes (Fig. 3).

With respect to MK801, although the frequency of neurites with lengths of 10–30 μm increased with increasing concentration of the agent, significance was not reached ($P > 0.05$,

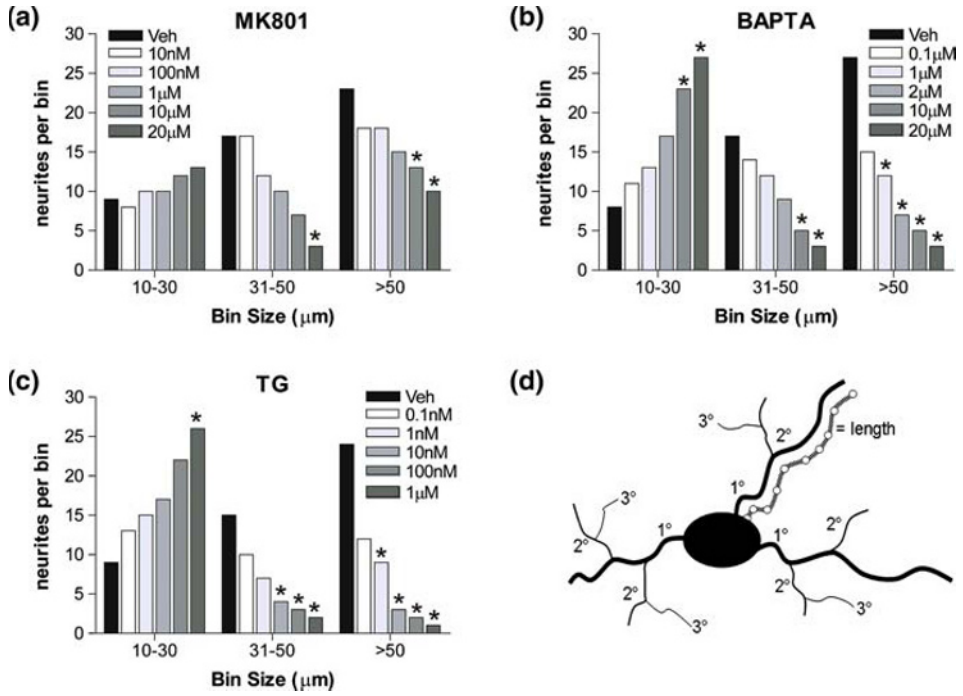

Fig. 3 Agent-induced decreases in neurite length. Neurons were grown for 1 DIV and exposed to varying concentrations of (**a**) MK801 (0.01–20 μM), (**b**) BAPTA (0.1–20 μM), or (**c**) thapsigargin (TG; 0.0001–1 μM) for 24 h. After fixing and staining for cytoskeletal markers (see Methods), neurite lengths were then estimated (see **d**) and data expressed as the number of neurites that fell into bin sizes 10–30 μm, 31–50 μm, or >50 μm in length. Differences between vehicle and treatment groups within a bin size were determined using χ^2 analysis (* significant at $P < 0.05$). (**d**) The length of each primary neurite was estimated by tracing the contours of rhodamine-phalloidin stained processes (stippled process illustrates procedure: at each turn of the neurite an anchor point was placed and the length of the resultant line was estimated; see Methods)

χ^2-test for trend; see also Fig. 3a). In contrast, in both the intermediate (31–50 μm) and larger (>50 μm) bin sizes, the frequency of neurites with such lengths decreased with increasing concentration of the agent, both of which reached significance ($P < 0.05$, χ^2-test for trend). Clearly, in the presence of MK801, neurite length was distributed in favor of smaller sizes. For BAPTA-treated cultures, we found that in the lower bin size the frequency of neurites increased with increased BAPTA concentration ($P < 0.05$, χ^2-test for trend; see also Fig. 3b), whereas in the intermediate and larger bin sizes the frequency of neurites decreased with increased BAPTA concentration ($P < 0.05$, χ^2-test for trend). Likewise, for TG-treated cultures, we found that in the lower bin size the frequency of neurites increased with increased TG concentration ($P < 0.05$, χ^2-test for trend; see also Fig. 3c), whereas in the intermediate and larger bin sizes the frequency of neurites decreased with increased TG concentration ($P < 0.05$, χ^2-test for trend). As with the growth cone analysis, both BAPTA and TG had more pronounced effects compared to MK801, with the order of potency being MK801 < BAPTA < TG. Because continued growth of these processes later leads to establishment of a formal network of fibers that facilitates the further maturation of cultures, inhibition of neurite growth at 1 DIV could interfere with long-term neuronal development (see Figs. 6 and 7).

Neurite Complexity

During early neuronal maturation, not only do neurites increase in length but they also increase in complexity, displaying numerous secondary and tertiary branching. As with the previous two studies, 1 DIV neurons were exposed to agents for 24 h, fixed and stained for the cytoskeletal marker F-actin (cultures were co-stained for tau or MAP2 as described in the previous section; not shown). Arborization of neuronal processes was quantified by determining the mean number of primary, secondary, and tertiary processes associated with each cell sampled in a given treatment group (see Methods).

In vehicle-treated wells, neurons displayed mostly primary neurites, with fewer secondary and fewer still tertiary neurites (Fig. 4). In MK801-treated wells, effect on neurite number was most evident in tertiary neurites, with all but the 10 nM concentrations yielding mean neurite numbers significantly lower than that found for vehicle (Fig. 4a). A similar action on secondary neurites was also observed, where neurite numbers declined with increasing concentration of MK801. However, NMDAR blockade reduced primary neurite numbers only at the 10 and 20 μM concentrations. In BAPTA-treated wells, a decline in the mean neurite number was observed at all concentrations for tertiary and secondary neurites but only at higher concentrations for primary neurites (Fig. 4b). In TG-treated wells, declines were observed at all concentrations for tertiary and secondary and all but 0.1 nM for primary neurites (Fig. 4c). Thus, the decline in neurite numbers was much more robust in the presence of TG compared to MK801 and BAPTA, with an order of potency of MK801 $<$ BAPTA $<$ TG. These results suggest that disrupting calcium homeostasis can inhibit neurite branching and arborization, an important phase in neuronal maturation that provides the substrate for later stages such as synaptogenesis.

Filopodial Extensions

In 1 DIV cultures, most processes had numerous short, slender filaments extending from the primary neurite shaft (filopodia; see Fig. 5). These extensions are thought to be the precursors of neurite branches or form new synapses with the processes of neighboring neurons (Williams et al. 1995; Chang and De Camilli 2001; Gibney and Zheng 2003; Portera-Cailliau et al. 2003). We therefore exposed 1 DIV neurons to vehicle or agents as described above and 24 h later determined the mean number of filopodia per unit length of primary neurite within each treatment group (see Methods). We found that in the vehicle-treated wells, primary neurites frequently displayed an abundance of filopodial extensions along the whole length of the process (see Fig. 5d, upper panel). However, in the presence of MK801, the mean number of filopodia per micron of neurite decreased with increasing concentration (Fig. 5a). Similarly, both BAPTA- (Fig. 5b) and TG-treated neurons (Fig. 5c) showed a loss of primary neurite filopodia with increasing concentration (see also Fig. 5d, lower panel). Again, as with other morphological features, TG had a much more dramatic effect on filopodia than MK801 or BAPTA. Given the roles that filopodia are thought to play in branching or neurite growth, these data suggest that inhibition of filopodia may precede agent-induced effects on other morphological features studied here.

Recovery of the Developmental Program

Having established that all 3 agents inhibit early neuronal maturation, we next wished to examine if cultures exposed to these agents after 1 DIV could recover and display

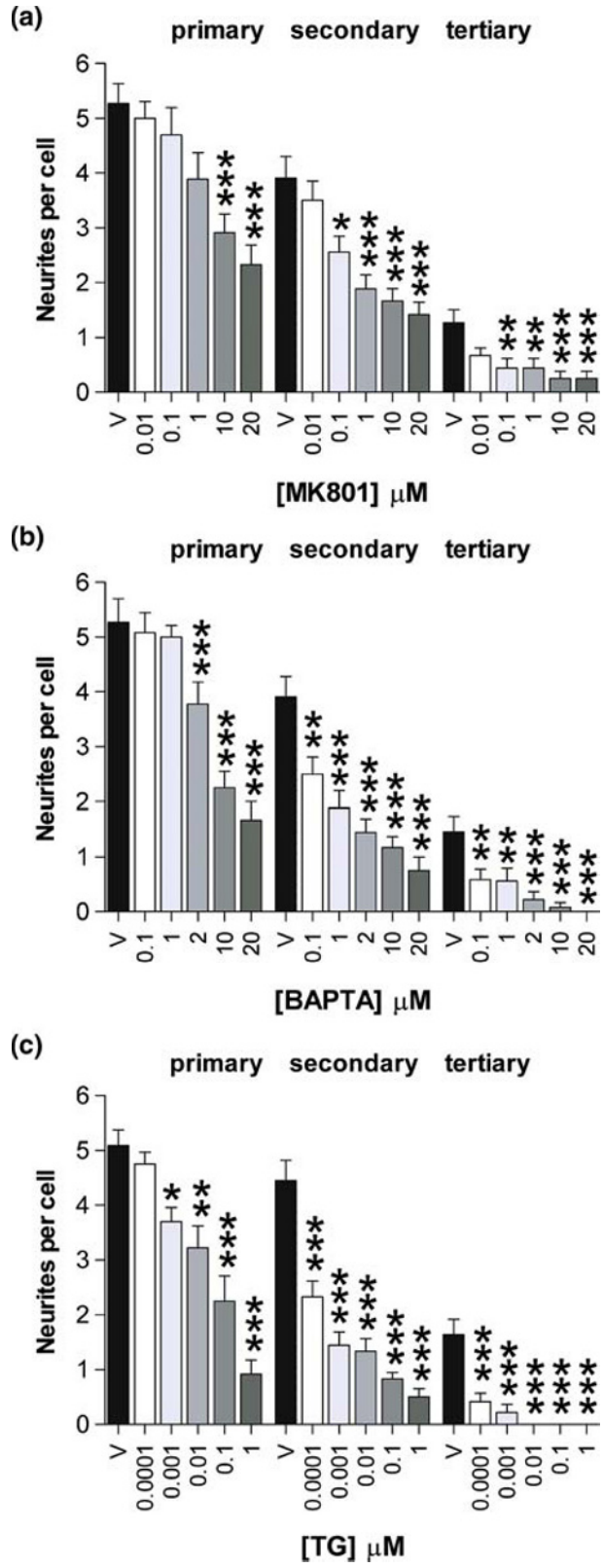

Fig. 4 Agent-induced loss of neurite complexity. Neurons were grown for 1 DIV and exposed to varying concentrations of (**a**) MK801 (0.01–20 μM), (**b**) BAPTA (0.1–20 μM), or (**c**) thapsigargin (TG; 0.0001–1 μM) for 24 h. After fixing and staining for cytoskeletal markers (see Methods), the mean number (±SE) of primary, secondary, or tertiary neurites per cell was estimated (See Methods and Fig. 3d for details). Differences between vehicle and treatment groups assessed by ANOVA using a Bonferroni post-test comparison of means (* $P < 0.05$; ** $P < 0.01$; *** $P < 0.001$)

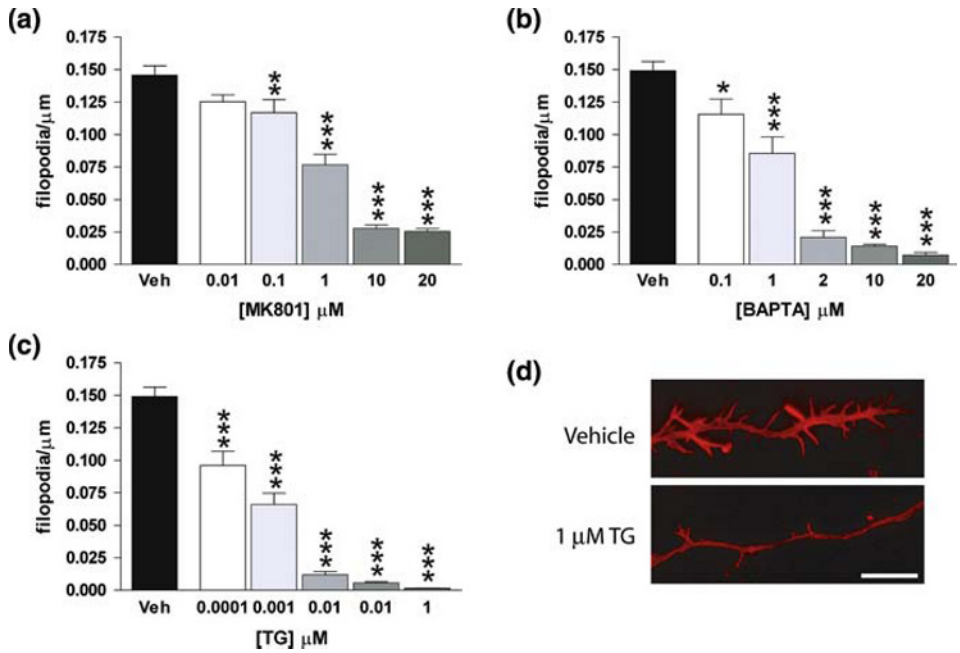

Fig. 5 Agent-induced decline in neurite-associated filopodia. Neurons were grown for 1 DIV and exposed to varying concentrations of (**a**) MK801 (0.01–20 μM), (**b**) BAPTA (0.1–20 μM), or (**c**) thapsigargin (TG; 0.0001–1 μM) for 24 h. After fixing and staining for cytoskeletal markers (see Methods), the mean number of filopodia per unit length of neurite (±SE) was then estimated and differences between treatment groups determined by ANOVA using a Bonferroni post-test comparison of means (* $P < 0.05$; ** $P < 0.01$; *** $P < 0.001$). (**d**) Top panel—neuronal process of vehicle-treated cell; bottom panel—neuronal process of TG-treated cell (1 μM); note the numerous filopodia in the top panel compared to the bottom panel. Scale bar in lower panel is 10 μm

morphological features found in agent-naïve cultures at later times. Thus, E18 embryonic cultures were grown for 1 DIV and then exposed to vehicle, MK801, BAPTA, or TG (using the same concentrations as above) for 24 h. After this time, all media was removed and quickly replaced with fresh media (this was done in sets of 4 wells each time, to avoid any drying out of the cultures). Cultures were then allowed to recover for either 4 DIV or 7 DIV, and fixed and stained for tau protein as described (see Methods).

The 4 and 7 DIV times were chosen because, in our experience, they represent discrete transitions in culture maturity. For example, at 4 DIV, vehicle-treated wells displayed low-fiber density, had processes that were easily distinguishable from each other, and had only a modest number of contacts (Fig. 6a). In contrast, at 7 DIV, vehicle-treated wells displayed high-fiber density, processes were not easily distinguishable from each other, and there were a higher number of contacts than observed at 4 DIV (Fig. 7a). Clearly, these two in vitro times represent distinct stages of network establishment and transition from one to the other would indicate that a long-term developmental program has been successfully engaged.

In 4 DIV cultures (previously exposed to MK801 at 1 DIV) there was a general trend toward loss of tau-positive fibers with increasing concentration, though significance was found only at 20 μM (Fig. 6b–d). However, at 7 DIV, significant loss of tau-ir fibers was observed at both the 10 and 20 μM concentrations (Fig. 7b–d). Given that we observed inhibition of development at 1 DIV with concentrations as low as 0.1 μM MK801, the data from the 4 and 7 DIV cultures suggest neurons are able to recover and follow a similar, albeit diminished, program of maturation as vehicle-treated controls. For BAPTA-treated wells, recovery at 4 DIV was severely

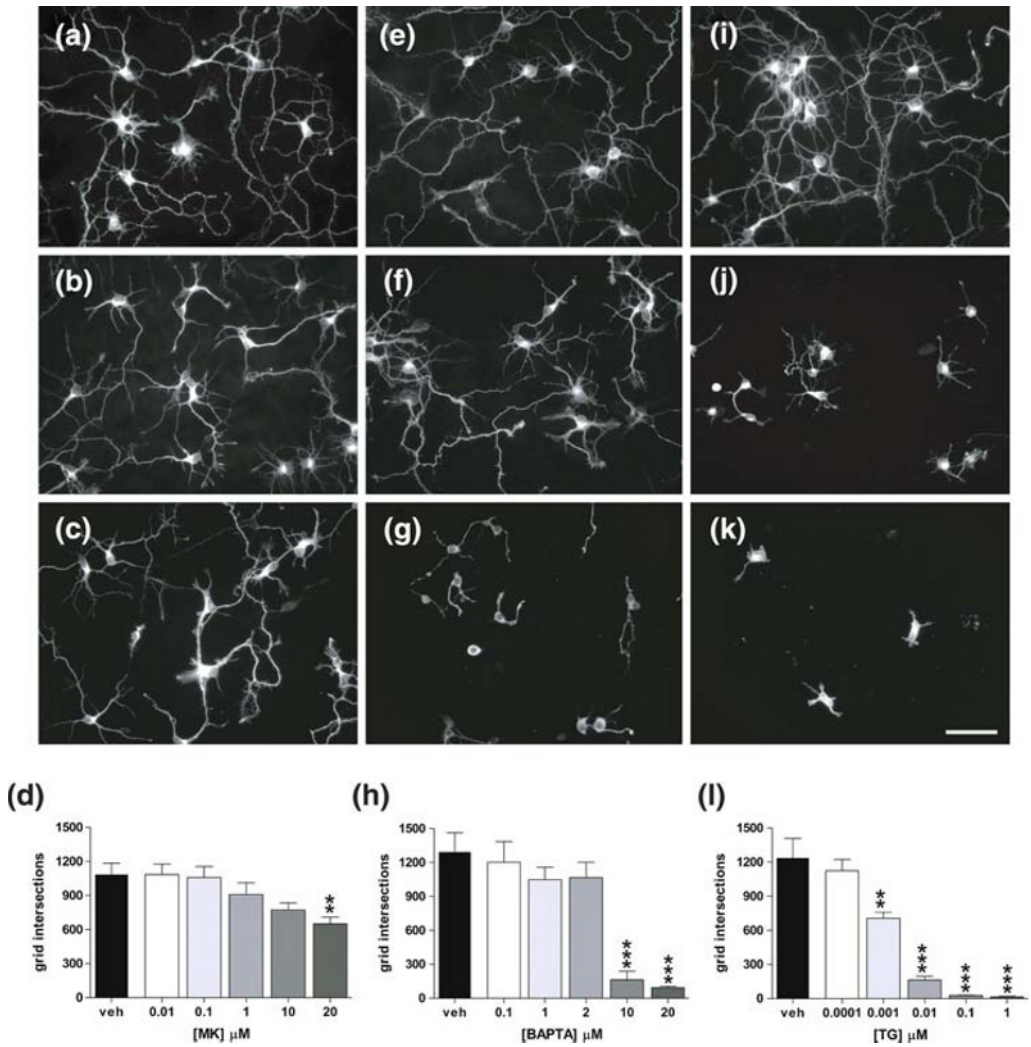

Fig. 6 Agent-induced inhibition of network development: 4 DIV. Neurons were grown for I DIV and exposed to vehicle or varying concentrations of MK801, BAPTA, or TG for 24 h, as described. Agents were then removed and cultures allowed to recover. At 4 DIV, cultures were fixed and stained for tau protein and the number of grid intersections made by tau-positive fibers estimated (see Methods). (**a–d**) Vehicle (**a**), 1 μM MK801 (**b**), or 20 μM MK801 (**c**); quantification of MK801 observations (**d**). (**e–h**) Vehicle (**e**), 2 μM BAPTA (**f**), or 20 μM BAPTA (**g**); quantification of BAPTA observations (**h**). (**i–l**) Vehicle (**i**), 10 nM TG (**j**), or 1 μM TG (**k**); quantification of TG observations (**l**). Scale bar in K is 30 μm. The mean number (±SE) of intersections per treatment group was determined and differences assessed by ANOVA using a Bonferroni post-test comparison of means (* $P < 0.05$; ** $P < 0.01$; *** $P < 0.001$)

reduced at 10 and 20 μM, and at 7 DIV recovery was modestly reduced at 2 μM and severely reduced at 10 and especially 20 μM. As with MK801, inhibition of development at 1 DIV was observed at concentrations lower than these, suggesting that recovery from low levels of BAPTA was also possible. For TG-treated wells, recovery at 4 DIV was modestly reduced at 1 nM and severely reduced at 10, 100 nM, and 1 μM (Fig. 6j–l). At 7 DIV, recovery was modestly to severely reduced at all concentrations (Fig. 7i–l). As with MK801 and BAPTA, TG inhibited neuronal development of 1 DIV cultures at lower concentrations but some recovery

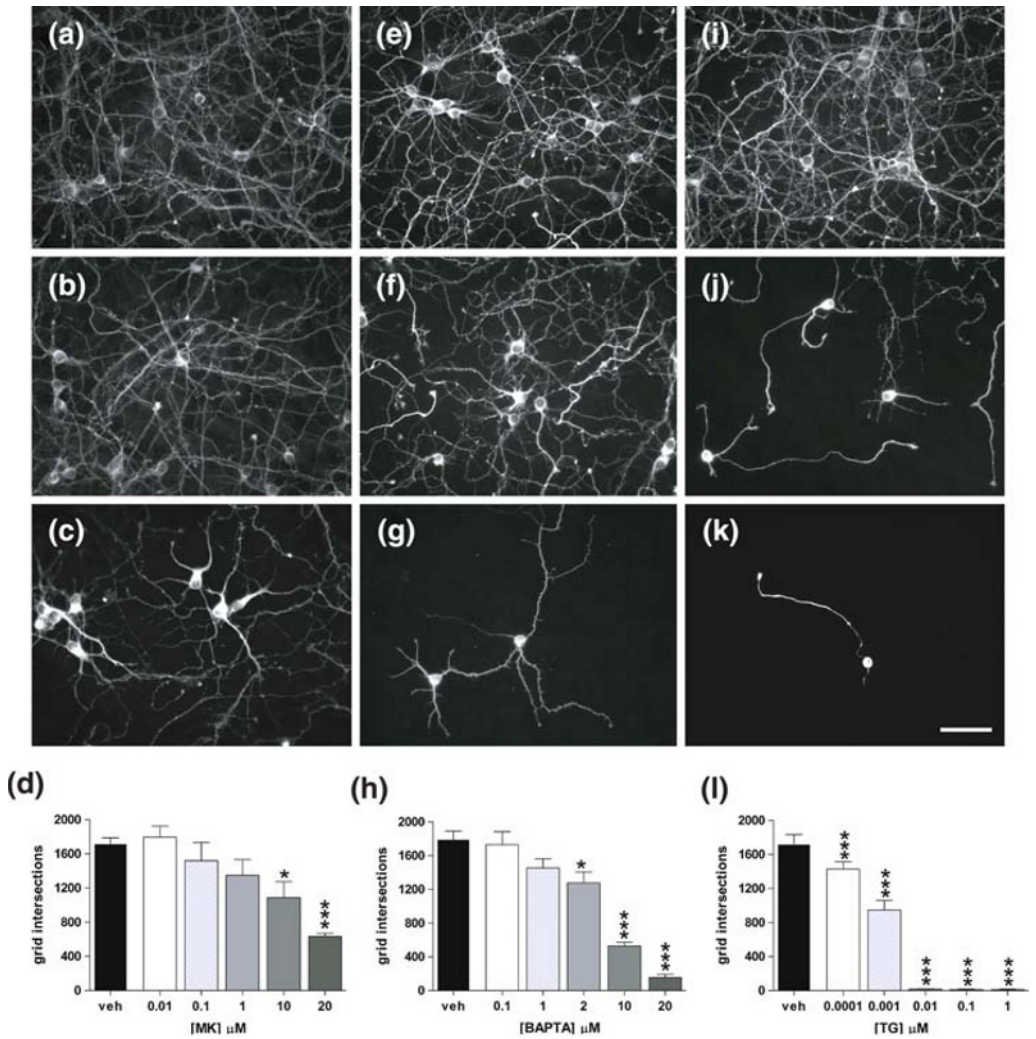

Fig. 7 Agent-induced inhibition of network development: 7 DIV. Neurons were grown for I DIV and exposed to vehicle or varying concentrations of MK801, BAPTA, or TG for 24 h, as described. Agents were then removed and cultures allowed to recover. At 7 DIV, cultures were fixed and stained for tau protein and the number of grid intersections made by tau-positive fibers estimated (see Methods). (**a–d**) Vehicle (**a**), 1 μM MK801 (**b**), or 20 μM MK801 (**c**); quantification of MK801 observations (**d**). (**e–h**) Vehicle (**e**), 2 μM BAPTA (**f**), or 20 μM BAPTA (**g**); quantification of BAPTA observations (**h**). (**i–l**) Vehicle (**i**), 10 nM TG (**j**), or 1 μM TG (**k**); quantification of TG observations (**l**). Scale bar in K is 30 μm. The mean number (±SE) of intersections per treatment group was determined and differences assessed by ANOVA using a Bonferroni post-test comparison of means (* $P < 0.05$; ** $P < 0.01$; *** $P < 0.001$)

was apparent at 4 DIV. However, by 7 DIV, neurons exposed to all concentrations of TG showed at least some loss of the normal developmental program.

Thus, using both 4 and 7 DIV recovery times was much more revealing than using one time only and showed that apparent recovery at 4 DIV may not be sustained at 7 DIV. Further, successful establishment of the development program was both concentration- and agent-dependent, with the order of recovery being MK801 > BAPTA > TG.

Potential Cytotoxic Action of Agents

To aid interpretation of our data, following exposure of 1 DIV neurons to vehicle or agents, we determined mean neuronal numbers after 24 h, 4 or 7 days later, as described (see Methods). In vehicle-treated wells, we observed a relatively constant number of neurons at each different in vitro time (Fig. 8), suggesting that neuronal number did not alter significantly with increasing time in culture, consistent with the post-mitotic nature of primary neurons. For MK801, we found that at each in vitro time, loss of neurons was observed at 10 and 20 μM (for all in vitro times). For BAPTA, a loss of neurons was observed at 10 and 20 μM (for all in vitro times) and was greater than that observed for MK801. For TG, loss of neurons was evident at 0.01–1 μM (for most in vitro times), and at 4 and 7 DIV, with neuronal loss greater still than MK801 or BAPTA. Therefore, whereas a cytotoxic effect was apparent for all three agents, the concentrations required for neuronal death were generally much higher than those needed to see the morphological changes described earlier.

Summary

Not only have we taken a comprehensive approach to studying the effects of agents on an array of morphological features associated with early neuronal development we have also examined effects of disrupting intracellular calcium in mechanistically different ways. Further, we have addressed both acute outcomes following disruption of calcium homeostasis as well as long-term effects as cultures mature. We show that neurons passing through the earliest stages of differentiation are highly sensitive to disruption of intracellular calcium. In addition, limited recovery from this early disruption was possible following NMDAR blockade or chelation of intracellular calcium. However, inhibiting the Ca^{2+}-ATPase pump had a much more dramatic effect on the ability of cultures to recover. These studies offer further insight into the role of calcium in neuronal development not only because of the comprehensive nature of the morphological features examined but also because we have compared both acute and long-term actions of three pharmacologically diverse agents.

Discussion

Calcium and Neuronal Maturation

Calcium levels within mature neurons are tightly regulated and calcium entry into a neuron or release from intracellular stores is thought to occur in a well-orchestrated manner (Berridge et al. 2000). However, the influence of calcium on events associated with neuronal development is very much context dependent as changes in intracellular calcium can elicit negative or positive responses depending on the route of entry, concentration of calcium at the time of change, or size of the calcium gradient (Gomez and Zheng 2006). Further, even the type of channel through which calcium may enter the neuron can differentially influence neurite growth and branching (Heng et al. 1999). Additionally, growth cones and their associated filopodia may be differentially sensitive to calcium compared to shaft filopodia (Davenport et al. 1996; Portera-Cailliau et al. 2003). Clearly, the status of the local environment as well as the nature of the local event may be factors that determine neuronal responses to changes in calcium.

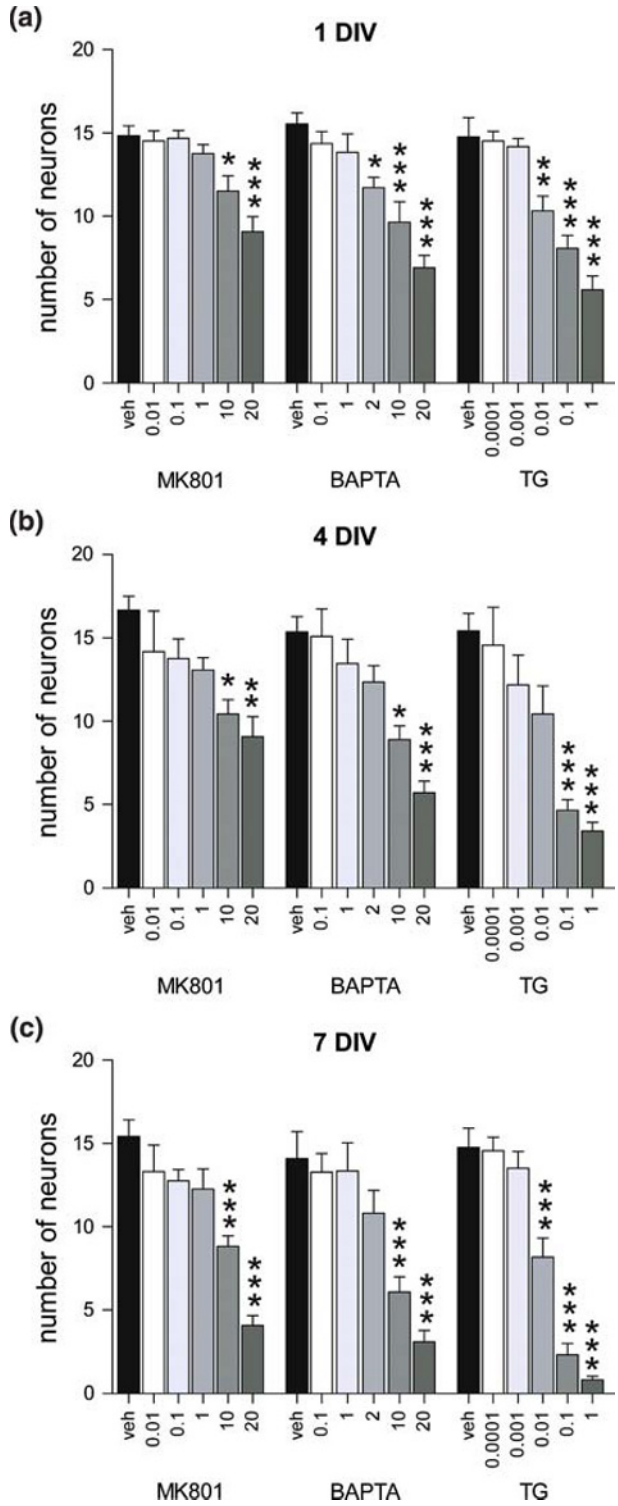

Fig. 8 Agent-induced neuronal death at various in vitro times. Neurons were grown for 1 DIV, exposed to agents for 24 h, and fixed immediately or allowed to recover and fixed at 4 DIV or 7 DIV. Cells were then stained for DAPI and large, weakly labeled nuclei were counted (presumptive neurons; see Fig. 1). (**a**) Cell counts 24 h post-exposure. (**b**) Cell counts at 4 DIV. (**c**) Cell counts at 7 DIV. The mean neuronal number (±SE) per treatment group was determined and differences assessed by ANOVA using a Bonferroni post-test comparison of means (* $P < 0.05$; ** $P < 0.01$; *** $P < 0.001$)

Whereas some studies suggest that reducing intracellular levels of calcium can promote growth cone motility and neurite extension (Tang et al. 2003), other studies suggest that lowering calcium inhibits these morphological features (Suarez-Isla et al. 1984; Mattson and Kater 1987; Cambray-Deakin and Burgoyne 1992), consistent with observations described here. However, even within the same study, both low and high neuronal calcium levels have been shown to induce growth cone collapse (Mattson and Kater 1987; Kater et al. 1988), suggesting that growth cone motility, as well as neurite growth and arborization, may require optimal levels of calcium, deviations above or below which result in negative outcomes. Similarly, neuronal survival may depend on maintaining a "calcium set point," first proposed by Eugene Johnson (Johnson et al. 1992) and later used by our group to explain neuronal death observed in P7 rats exposed to MK801 (Turner et al. 2002; Turner et al. 2007a; Turner et al. 2007b). Indeed, more recently we have shown that MK801-induced injury in P7 rats is observed in cells that lack the CaBPs calbindin-D28K, calretinin, or parvalbumin (Lema Tomé et al. 2006). Thus, changes in neuronal calcium may drive neuronal survival and maturation or initiate cell death pathways, depending on the status of intracellular calcium within the whole neuron or subcellular region under study (Mattson 1992).

Network Establishment

Having shown morphological changes after agent exposure at 1 DIV, we felt an important question to ask was whether neurons could still continue on with their developmental program and establish connections with each other. Thus, whereas MK801-treated cultures showed clear inhibition of growth cones and neurites at 1 DIV, examination of such cultures at 4 and 7 DIV suggested that the inhibition was not permanent and recovery was possible, at least at the lower concentrations. Likewise, BAPTA-treated cultures also displayed signs of inhibition at 1 DIV with recovery of the normal developmental program at later times, albeit more limited compared to MK801. However, it was clear that not only was TG quite potent at inhibiting neuronal maturation at 1 DIV but also recovery from such inhibition was less likely than that found for either MK801 or BAPTA, suggesting that developing neurons can locate alternative sources of calcium when calcium entry or cytosolic calcium is not optimal.

The action of BAPTA appeared to fall in between the effects of MK801 and TG. For example, lower concentrations of BAPTA more closely mirrored MK801 action, resulting in only mild inhibition of growth cones and neurites, whereas higher concentrations of BAPTA produced outcomes more comparable to TG. Perhaps at low BAPTA concentrations chelation-induced changes in calcium fall within a physiological range, mimicking natural buffering of this ion by CaBPs, and so recovery was possible. At higher BAPTA concentrations, calcium chelation is more robust, taking calcium levels well outside any physiological range, and pathological effects become apparent (indeed, we have previously noted abrupt increases in cell death when transitioning from low to high BAPTA concentrations (Turner et al. 2007a)).

Because calcium is pivotal to neuronal maturation and survival (Johnson et al. 1992; Mattson 1992; Berridge et al. 2000), neurons that can regulate calcium efficiently may survive and succeed in making functional connections with other neurons. However, subpopulations of neurons less able to regulate internal calcium may be intrinsically more sensitive to agent- (or event)-induced changes in this ion (Lema Tomé et al. 2006, 2007). Alternatively, the manner in which neuronal calcium is disrupted may be critical in determining if the normal developmental program is affected. Given that distinct pools of calcium are networked across the

cell, it is likely that disrupting calcium homeostasis at one focal point will have ripple effects across such a network. What would be of interest in future studies from this lab is to determine which of these pools are more important to developing neurons.

Regulation of Neuronal Maturation by NMDA Receptors

Although previous studies strongly suggest glutamate regulates early in vitro neuronal development (Pearce et al. 1987; Burgoyne et al. 1988; Brewer and Cotman 1989; Rashid and Cambray-Deakin 1992; Zheng et al. 1996; Cuppini et al. 1999; Heng et al. 1999; Chang and De Camilli 2001), NMDARs are thought not to be fully expressed (Zhong et al. 1994; Li et al. 1998) or functional (Murphy and Baraban 1990; Ujihara and Albuquerque 1992) until 7 DIV. However, other studies suggest that NMDAR subunits are indeed present as early as 1 DIV (Pearce et al. 1987; Allen et al. 1988; Zhong et al. 1994; Heng et al. 1995; Lin et al. 1997; Li et al. 1998; Cuppini et al. 1999) and are thought to be functional (Cuppini et al. 1999). We have confirmed the presence of the obligatory NR1 subunit (see Fig. 1) and found that MK801 inhibits NMDA-induced increases in expanded growth cones (see Results). Thus, we feel that the MK801 action on growth cones, as well as neurite length and complexity, was mediated through the NMDAR.

Our data suggest that blockade of the NMDAR by MK801 can inhibit neuronal development but that recovery was possible, at least at the lower concentrations. Thus, although this agent can induce robust apoptosis in neonatal animals (Ikonomidou et al. 1999; Turner et al. 2002; Turner et al. 2007b), the data we now present suggest more subtle effects may also occur, which include inhibition of the developmental program of MK801-sensitive neurons. A critical question that remains is whether MK801 promotes cell death independent of inhibition of neuronal maturation or does such inhibition actually initiate cell death? Our in vitro data show that inhibition is observed at lower concentrations but that cell death occurs only at the highest concentrations, suggesting inhibition is a primary event that may be followed later by cell death. We hope future studies will shed more light on this intriguing question.

Implications for In Vivo Studies

P7 rat pups treated with MK801 display robust apoptosis in multiple brain regions (Ikonomidou et al. 1999; Lema Tomé et al. 2006; Turner et al. 2007b), suggesting significant rewiring of the CNS should be expected. However, not only do these animals survive but they also appear to be, in a general sense, behaviorally normal, suggesting that essential CNS circuits remain intact or are plastic enough to recover from MK801-induced injury. Nevertheless, at later ages these animals do exhibit specific behavioral deficits (Harris et al. 2003), suggesting recovery of CNS circuits may be incomplete or compromised. Likewise, here we have shown that, following early exposure to MK801, a network can be established at later in vitro times, though in a more limited manner compared to vehicle controls. Thus, future studies may reveal that early exposure of neurons to agents that disrupt calcium homeostasis will still produce viable networks but intrinsic or evoked activity within the network may be substantially altered.

Summary

We have examined both acute (24 h) and long-term (4 and 7 DIV) effects of 3 agents that alter intracellular calcium in mechanistically different ways. Our observations on the acute effects

of these agents both confirm as well as add considerably to the work of others. However, we have extended these findings by demonstrating that MK801, BAPTA, and TG can also influence long-term development of neurons. There are now many drugs used in obstetrics or neonatology to control blood pressure or induce anesthesia which act by altering neuronal calcium. Our data suggest that maintenance of calcium homeostasis should be considered as a preventative strategy to limit potential brain injury when exposing fetuses or young children to such drugs.

Acknowledgments We are grateful for the technical support of Carla Lema Tomé. This work was supported by a Wake Forest University School of Medicine Faculty Development fund, a Mr and Mrs Tab Williams Jr and Family Neuroscience Research and Program Development Endowment, and NIH RO1 NS051632. Tissue culture procedures, imaging, and data analysis were performed by SLR, JA, EB, MA, and CPT. Manuscript and figures prepared by SLR, JA, and CPT. There are no conflicting interests for all authors.

References

Allen CN, Brady R, Swann J, Hori N, Carpenter DO (1988) *N*-methyl-D-aspartate (NMDA) receptors are inactivated by trypsin. Brain Res 458:147–150

Berridge MJ, Lipp P, Bootman MD (2000) The versatility and universality of calcium signalling. Nat Rev Mol Cell Biol 1:11–21

Bradke F, Dotti CG (1999) The role of local actin instability in axon formation. Science 283:1931–1934

Bradke F, Dotti CG (2000) Differentiated neurons retain the capacity to generate axons from dendrites. Curr Biol 10:1467–1470

Brewer GJ, Cotman CW (1989) NMDA receptor regulation of neuronal morphology in cultured hippocampal neurons. Neurosci Lett 99:268–273

Burgoyne RD, Pearce IA, Cambray-Deakin M (1988) *N*-methyl-D-aspartate raises cytosolic calcium concentration in rat cerebellar granule cells in culture. Neurosci Lett 91:47–52

Cambray-Deakin MA, Burgoyne RD (1992) Intracellular Ca^{2+} and *N*-methyl-D-aspartate-stimulated neuritogenesis in rat cerebellar granule cell cultures. Brain Res Dev Brain Res 66:25–32

Chang S, De Camilli P (2001) Glutamate regulates actin-based motility in axonal filopodia. Nat Neurosci 4:787–793

Cheng C, Fass DM, Reynolds IJ (1999) Emergence of excitotoxicity in cultured forebrain neurons coincides with larger glutamate-stimulated [Ca(2+)](i) increases and NMDA receptor mRNA levels. Brain Res 849: 97–108

Chilton JK, Gordon-Weeks PR (2006) Role of microtubules and MAPs during neuritogenesis. In: de Curtis I (ed) Intracellular mechanisms for neuritogenesis. Springer, Milan, pp 57–88

Cuppini R, Sartini S, Ambrogini P, Falcieri E, Maltarello MC, Gallo G (1999) Control of neuron outgrowth by NMDA receptors. J Submicrosc Cytol Pathol 31:31–40

Davenport RW, Dou P, Mills LR, Kater SB (1996) Distinct calcium signaling within neuronal growth cones and filopodia. J Neurobiol 31:1–15

Dotti CG, Sullivan CA, Banker GA (1988) The establishment of polarity by hippocampal neurons in culture. J Neurosci 8:1454–1468

Fletcher TL, Banker GA (1989) The establishment of polarity by hippocampal neurons: the relationship between the stage of a cell's development in situ and its subsequent development in culture. Dev Biol 136: 446–454

Fletcher TL, De Camilli P, Banker G (1994) Synaptogenesis in hippocampal cultures: evidence indicating that axons and dendrites become competent to form synapses at different stages of neuronal development. J Neurosci 14:6695–6706

Gallo G, Letourneau PC (1999) Axon guidance: a balance of signals sets axons on the right track. Curr Biol 9:R490–R492

Gibney J, Zheng JQ (2003) Cytoskeletal dynamics underlying collateral membrane protrusions induced by neurotrophins in cultured Xenopus embryonic neurons. J Neurobiol 54:393–405

Gomez TM, Zheng JQ (2006) The molecular basis for calcium-dependent axon pathfinding. Nat Rev Neurosci 7:115–125

Harris LW, Sharp T, Gartlon J, Jones DN, Harrison PJ (2003) Long-term behavioural, molecular and morphological effects of neonatal NMDA receptor antagonism. Eur J Neurosci 18:1706–1710

Heng JE, Moscaritolo K, Dreyer EB (1995) NMDA sensitivity is neurite enhanced. Neuroreport 6:1890–1892

Heng JE, Zurakowski D, Vorwerk CK, Grosskreutz CL, Dreyer EB (1999) Cation channel control of neurite morphology. Brain Res Dev Brain Res 113:67–73

Herschkowitz N (1988) Brain development in the fetus, neonate and infant. Biol Neonate 54:1–19

Hoffmann H, Gremme T, Hatt H, Gottmann K (2000) Synaptic activity-dependent developmental regulation of NMDA receptor subunit expression in cultured neocortical neurons. J Neurochem 75:1590–1599

Ikonomidou C, Bosch F, Miksa M, Bittigau P, Vockler J, Dikranian K, Tenkova TI, Stefovska V, Turski L, Olney JW (1999) Blockade of NMDA receptors and apoptotic neurodegeneration in the developing brain. Science 283:70–74

Johnson EM Jr, Koike T, Franklin J (1992) A "calcium set-point hypothesis" of neuronal dependence on neurotrophic factor. Exp Neurol 115:163–166

Kater SB, Mattson MP, Cohan C, Connor J (1988) Calcium regulation of the neuronal growth cone. Trends Neurosci 11:315–321

Lema Tomé CM, Miller R, Bauer C, Nottingham C, Smith C, Blackstone K, Brown L, Bryan R, Leigh A, Brady M, Busch J, Turner CP (2007) Decline in age-dependent MK801-induced injury coincides with developmental surge in parvalbumin expression: cingulate and retrosplenial cortex. Dev Psychobiol 49:606–618

Lema Tomé CM, Bauer C, Nottingham C, Smith C, Blackstone K, Brown L, Hlavaty C, Nelson C, Daker R, Sola R, Miller R, Bryan R, Turner CP (2006) MK801-induced caspase-3 in the postnatal brain: Inverse relationship with calcium binding proteins. Neuroscience 141:1351–1363

Levitt P (2003) Structural and functional maturation of the developing primate brain. J Pediatr 143:S35–S45

Li JH, Wang YH, Wolfe BB, Krueger KE, Corsi L, Stocca G, Vicini S (1998) Developmental changes in localization of NMDA receptor subunits in primary cultures of cortical neurons. Eur J Neurosci 10:1704–1715

Lin WW, Wang CW, Chuang DM (1997) Effects of depolarization and NMDA antagonists on the role survival of cerebellar granule cells: a pivotal role for protein kinase C isoforms. J Neurochem 68:2577–2586

Mattson MP (1992) Calcium as sculptor and destroyer of neural circuitry. Exp Gerontol 27:29–49

Mattson MP, Kater SB (1987) Calcium regulation of neurite elongation and growth cone motility. J Neurosci 7:4034–4043

Ming Z, Griffith BL, Breese GR, Mueller RA, Criswell HE (2002) Changes in the effect of isoflurane on *N*-methyl-D-aspartic acid-gated currents in cultured cerebral cortical neurons with time in culture: evidence for subunit specificity. Anesthesiology 97:856–867

Murphy TH, Baraban JM (1990) Glutamate toxicity in immature cortical neurons precedes development of glutamate receptor currents. Brain Res Dev Brain Res 57:146–150

Pearce IA, Cambray-Deakin MA, Burgoyne RD (1987) Glutamate acting on NMDA receptors stimulates neurite outgrowth from cerebellar granule cells. FEBS Lett 223:143–147

Portera-Cailliau C, Pan DT, Yuste R (2003) Activity-regulated dynamic behavior of early dendritic protrusions: evidence for different types of dendritic filopodia. J Neurosci 23:7129–7142

Ramoa AS, Alkondon M, Aracava Y, Irons J, Lunt GG, Deshpande SS, Wonnacott S, Aronstam RS, Albuquerque EX (1990) The anticonvulsant MK-801 interacts with peripheral and central nicotinic acetylcholine receptor ion channels. J Pharmacol Exp Ther 254:71–82

Rashid NA, Cambray-Deakin MA (1992) *N*-methyl-D-aspartate effects on the growth, morphology and cytoskeleton of individual neurons in vitro. Brain Res Dev Brain Res 67:301–308

Rice D, Barone S Jr (2000) Critical periods of vulnerability for the developing nervous system: evidence from humans and animal models. Environ Health Perspect 108(Suppl 3):511–533

Santama N, Dotti CG, Lamond AI (1996) Neuronal differentiation in the rat hippocampus involves a stage-specific reorganization of subnuclear structure both in vivo and in vitro. Eur J Neurosci 8:892–905

Suarez-Isla BA, Pelto DJ, Thompson JM, Rapoport SI (1984) Blockers of calcium permeability inhibit neurite extension and formation of neuromuscular synapses in cell culture. Brain Res 316:263–270

Takashima S, Iida K, Deguchi K (1995) Periventricular leukomalacia, glial development and myelination. Early Hum Dev 43:177–184

Tang F, Dent EW, Kalil K (2003) Spontaneous calcium transients in developing cortical neurons regulate axon outgrowth. J Neurosci 23:927–936

Tucker LM, Morton AJ (1995) A simple method for quantifying changes in neuronal populations in primary cultures of dissociated rat brain. J Neurosci Methods 59:217–223

Turner CP, Pulciani D, Rivkees SA (2002) Reduction in intracellular calcium levels induces injury in developing neurons. Exp Neurol 178:21–32

Turner CP, Connell J, Blackstone K, Ringler SL (2007a) Loss of calcium and increased apoptosis within the same neuron. Brain Res 1128:50–60

Turner CP, Miller R, Smith C, Brown L, Blackstone K, Dunham SR, Strehlow R, Manfredi M, Slocum P, Iverson K, West M, Ringler SL, Berry ZC (2007b) Widespread neonatal brain damage following calcium channel blockade. Dev Neurosci 29:213–231

Ujihara H, Albuquerque EX (1992) Ontogeny of *N*-methyl-D-aspartate-induced current in cultured hippocampal neurons. J Pharmacol Exp Ther 263:859–867

Williams CV, Davenport RW, Dou P, Kater SB (1995) Developmental regulation of plasticity along neurite shafts. J Neurobiol 27:127–140

Zheng JQ, Wan JJ, Poo MM (1996) Essential role of filopodia in chemotropic turning of nerve growth cone induced by a glutamate gradient. J Neurosci 16:1140–1149

Zhong J, Russell SL, Pritchett DB, Molinoff PB, Williams K (1994) Expression of mRNAs encoding subunits of the *N*-methyl-D-aspartate receptor in cultured cortical neurons. Mol Pharmacol 45:846–853

Zhong J, Carrozza DP, Williams K, Pritchett DB, Molinoff PB (1995) Expression of mRNAs encoding subunits of the NMDA receptor in developing rat brain. J Neurochem 64:531–539